Direct Measurement of Singlet−Triplet Splitting within Rodlike Photogenerated Radical Ion Pairs Using Magnetic Field Effects: Estimation of the Electronic Coupling for Charge Recombination

Emily A. Weiss, Mark A. Ratner,* and Michael R. Wasielewski*

Department of Chemistry and Center for Nanofabrication and Molecular Self-Assembly, Northwestern University, Evanston, Illinois 60208-3113

Determining the electronic coupling matrix element, *V*, for an electron transfer reaction is challenging both experimentally and theoretically. The magnitude of the singlet−triplet splitting (spin−spin exchange interaction), 2*J*, within a radical ion pair (RP) is directly related to the sum of the squares of the matrix elements that couple the RP state to the ground state and to other energetically proximate excited and ionic states. Each term in this sum is weighted by the reciprocal of the energy gap between the RP state and the particular state to which it is coupled. We present here a series of intramolecular triads with linear, rodlike structures that undergo very efficient two-step electron transfer following direct excitation of a 4-(*N*-piperidinyl)naphthalene-1,8-dicarboximide (6ANI) chromophore. Attachment of a *p*-methoxyaniline (MeOAn) donor by means of the piperazine bridge and naphthalene-1,8:4,5-bis(dicarboximide) (NI) or pyromellitimide (PI) acceptors, either directly or through a 2,5-dimethylphenyl (Me$_2$Ph) spacer to 6ANI results in the triads MeOAn-6ANI-NI, MeOAn-6ANI-PI, MeOAn-6ANI-Me$_2$Ph-NI, and MeOAn-6ANI-Me$_2$Ph-PI. The two-step charge separation from the lowest excited singlet state of 6ANI yields singlet radical ion pairs in which the charges are separated by 14 to 19 Å and whose lifetimes range from about 15 to 200 ns. These lifetimes are long enough such that radical pair intersystem crossing occurs to form the triplet radical ion pair, which then recombines to form the ground state and a neutral excited triplet state, which is localized either on 6ANI or NI. The yield of this locally excited triplet state, monitored by nanosecond transient absorption as a function of applied magnetic field strength, exhibits distinct resonances that directly yield 2*J*. The value of 2*J* is used to estimate *V*$_{CR}$ for charge recombination of the radical ion pair. These measurements provide a highly sensitive method of determining the dependence of the electronic coupling on the structure of the radical ion pair.

Introduction

One of the most important issues that arises in designing molecular systems to photochemically separate and store charge efficiently is how molecular structure controls the electronic coupling matrix elements, *V*$_{CR}$, for the energy wasting charge recombination reactions. Theory has shown that the singlet−triplet splitting within the radical ion pair (RP), given by the magnitude of the singlet−triplet splitting (spin−spin exchange interaction), 2*J*, between the two unpaired electrons, is a weighted sum of the squares of the matrix elements that couple the RP state to the ground state and to locally excited states on the donor and acceptor.[1−9] Thus, a direct measurement of 2*J* can be used to estimate *V*$_{CR}$. This paper describes a series of rodlike donor−acceptor molecules in which 2*J* is measured directly by observing resonances in the magnetic field effect on the yields of the molecular triplet state produced when the initially formed singlet radical ion pair (RP) undergoes radical pair intersystem crossing (RP-ISC) to the triplet RP followed by charge recombination. Changes in the magnitude of 2*J* as well as in the number and line shapes of the 2*J* resonances can be directly correlated with radical ion pair structure. The relationship between 2*J* and the electronic coupling matrix element for charge recombination, *V*$_{CR}$, makes it possible to

probe the dependence of *V*$_{CR}$ on subtle changes in molecular structure at an unprecedented level of detail, thereby providing insights into how to optimize structures for efficient electron transfer.

The rates of nonadiabatic charge recombination reactions, *k*$_{CR}$, depend critically on their corresponding off-diagonal, charge transfer (CT) elements of the full electronic Hamiltonian, *V*$_{CR}$

$$k_{CR} = \frac{2\pi}{\hbar}|V_{CR}{}^2|(\text{FCWD}) \qquad (1)$$

where FCWD is the Franck−Condon weighted density of states.[10] Calculations of the magnitudes of indirect superexchange coupling have been based on both ab initio and semiempirical schemes,[11−17] but for long-range, many-site coupling, ab initio methods are difficult, and semiempirical methods often use Hamiltonians not parametrized to predict the desired properties. A direct experimental determination of this quantity is desirable to provide important insights into the mechanisms of electron transfer within complex systems. Such mechanistic understanding is needed for testing both new and established theoretical methods and for the design of donor−acceptor arrays for molecular devices based on efficient charge separation.

A series of rodlike molecules consisting of aromatic imide and diimide donors and acceptors linked directly or through a

* To whom correspondence should be addressed.

3640 *J. Phys. Chem. A, Vol. 107, No. 19, 2003*

Weiss et al.

2,5-dimethylphenyl spacer have been synthesized to map the influence of structural and electronic characteristics on V_{CR}. Specifically, radical ion pairs (RPs) are created in these triads through charge separation reactions from the photoexcited singlet state of their common chromophore, 4-(*N*-piperidinyl)-naphthalene-1,8-dicarboximide (6ANI).[18] These RPs are initially formed in rapid, nonadiabatic reactions to produce a singlet RP, $^1(D^+A^-)$, which can then either recombine to the ground-state singlet, (DA), or intersystem cross to the triplet RP, $^3(D^+A^-)$, through a mechanism effected by local electron−nuclear hyperfine and electron spin−spin exchange interactions.

The efficiency of singlet−triplet (S−T) mixing within the RP depends on the magnitude of the splitting between the singlet and triplet RP states, $2J$, which is nonzero due to isotropic net ferromagnetic/antiferromagnetic exchange between the two unpaired electrons. Although direct, ferromagnetic exchange predicts a parallel orientation of two magnetic spins because of the elimination of same-site Coulomb repulsion, the direct interaction is negligible for a well-separated RP, for which the dominant contribution to $2J$ is the virtual transfer of the electron from the anion to an empty orbital on the donor cation.[19] This virtual transfer amounts to interaction of the RP state with ground and localized excited states.

In 1959, Anderson,[1] considering solid insulators, used a perturbational approach to relate the singlet−triplet splitting of a two-spin system to the magnitude of the electron-transfer superexchange coupling, V_{RP-n}, between the radical ion pair state and surrounding states n

$$2J = E_S - E_T = \left[\sum_n \frac{|\langle \Psi_{RP}|V_{RP-n}|\Psi_n\rangle|^2}{\Delta E_{RP-n}}\right]_S - \left[\sum_n \frac{|\langle \Psi_{RP}|V_{RP-n}|\Psi_n\rangle|^2}{\Delta E_{RP-n}}\right]_T \quad (2)$$

where $\Delta E_{RP-n} = E_{RP} - E_n - \lambda$ is the energy gap between the RP state and that state to which it is coupled at the nuclear coordinate of the relaxed RP state and λ is the vertical reorganization energy for the electron transfer. The individual terms in eq 2 may be ferromagnetic or antiferromagnetic depending on the sign of the energy denominator.

In the case of net antiferromagnetic exchange, the lowest energy configuration of the RP is a singlet with an S−T splitting equal to the weighted sum of the squares of the electronic coupling matrix elements as given by eq 2. This splitting can be measured with high sensitivity in donor−acceptor systems where the spin−spin exchange interaction is sufficiently small to allow the RP to intersystem cross to form the triplet RP. The singlet and triplet RPs then combine spin-selectively to form, respectively, the neutral ground-state singlet and lowest excited triplet state localized on either the donor or acceptor. This radical pair mechanism (RPM) is well-known to account for triplet production within photosynthetic reaction centers[20−33] and is marked by a sensitivity of the yield of localized triplet to the application of an external magnetic field, which splits the triplet RP manifold into its Zeeman sublevels, modulating the efficiency of S−T mixing.

This paper describes the use of magnetic field effects on the yield of the triplet state produced by the RPM and monitored by nanosecond transient optical absorption spectroscopy to measure $2J$ in photogenerated RP's within rigid rodlike arrays composed of a *p*-methoxyaniline (MeOAn) donor, a 4-(*N*-piperidinyl)naphthalene-1,8-dicarboximide (6ANI) chromophore,

CHART 1: Structures of Donor−Accpetor Molecules

MeOAn-6ANI-NI

MeOAn-6ANI-PI

MeOAn-6ANI-Me$_2$Ph-NI

MeOAn-6ANI-Me$_2$Ph-PI
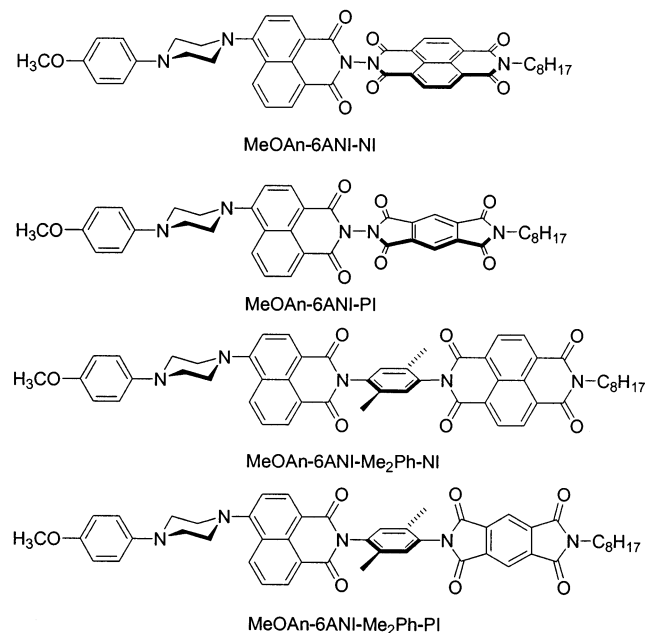
that can act as either a donor or an acceptor, and either 1,8:4,5-naphthalenediimide (NI) or pyromellitimide (PI) secondary acceptors, Chart 1. The charge recombination to the localized triplet states within these systems is expected to be a dominant contributor to $2J$ because the energy gaps between the RP states and the recombination triplets are relatively small. The matrix element for charge recombination, V_{CR}, is estimated using eq 2 and is discussed with respect to donor−acceptor distance (r_{DA}) and orientation. The line shape of the magnetic field effect on the triplet yield is related to the strength of the hyperfine interaction and the degree of charge delocalization on each radical center.
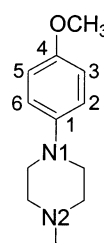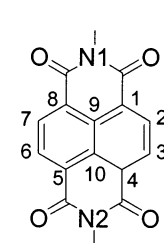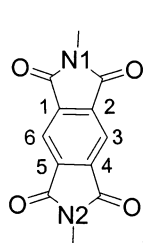
Experimental Section

The synthesis and characterization of compounds MeOAn-6ANI-PI[34] and MeOAn-6ANI-Me$_2$Ph-NI[18] have been reported previously, and that of MeOAn-6ANI-NI and MeOAn-6ANI-Me$_2$Ph-PI can be found in the Supplementary Information. Characterization was performed with a Gemini 300 MHz, Varian 400 MHz, or INOVA 500 MHz NMR and a PE BioSystems MALDI-TOF mass spectrometer. All solvents were spectrophotometric grade or distilled prior to use.

Cyclic voltammetry measurements were performed in butyronitrile solution containing 0.1 M tetra-*n*-butylammonium perchlorate electrolyte using a CH model 622 electrochemical work station. A 1.0 mm diameter platinum disk electrode, platinum wire counter electrode, and Ag/Ag$_x$O reference electrode were employed. The ferrocene/ferrocinium couple (Fc/Fc$^+$, 0.52 vs SCE) was used as an internal reference for all measurements.

Absorption measurements were made on a Shimadzu (UV-1601) spectrophotometer. The optical density of all samples was maintained between 0.7 and 1.0 at 416 nm, ($\epsilon_{6ANI,416\,nm} = 7000$ cm^{-1} M^{-1}).[18] Femtosecond transient absorption measurements were made using the 420 nm frequency-doubled output from a regeneratively amplified titanium sapphire laser system operating at 2 kHz as the excitation pulse.[35] Samples were placed in a 2 mm path length quartz cuvette and stirred using a motorized wire stirrer. Nanosecond transient absorption measurements were made using the 416 nm, H$_2$−Raman shifted output from a

Direct Measurement of Singlet−Triplet Splitting

J. Phys. Chem. A, Vol. 107, No. 19, 2003 **3641**

CHART 2: Radical Ion Spin Densities Calculated Using the UHF-AM1 Method

	ρ
1	-0.151
2	0.350
3	-0.264
4	0.386
5	-0.248
6	0.295
O	0.096
N1	0.528
N2	0.011

	ρ
1	0.230
2	0.052
3	0.052
4	0.230
5	0.230
6	0.052
7	0.052
8	0.230
9	-0.137
10	-0.137

	ρ
1	0.308
2	0.308
3	-0.243
4	0.308
5	0.308
6	-0.243

frequency-tripled 10-Hz Nd:YAG laser (QuantaRay DCR-2). Samples were placed in a 10 mm path length quartz cuvette equipped with a vacuum adapter and subjected to five freeze−pump−thaw degassing cycles prior to transient absorption measurements. The probe light in the nanosecond experiments was generated using a xenon flashlamp (EG&G Electrooptics FX-200) and detected using a photomultiplier tube with high voltage applied to only 4 dynodes (Hamamatsu R928). The total instrument response is 7 ns and is determined primarily by the laser pulse duration. The sample cuvette was placed between the poles of a Walker Scientific HV-4W electromagnet powered by a Walker Magnion HS-735 power supply. The field strength was measured by a Lakeshore 450 gaussmeter with a Hall effect probe. Both the electromagnet and the gaussmeter were interfaced with the data collection computer, allowing measurement and control of the magnetic field to $\pm 1 \times 10^{-5}$ T during data acquisition.

Kinetic traces for MeOAn-6ANI-NI, MeOAn-6ANI-PI, and MeOAn-6ANI-Me$_2$Ph-PI were recorded over a range of 1 μs, whereas those for MeOAn-6ANI-Me$_2$Ph-NI were over a range of 2 μs. Between 50 and 80 shots were averaged at each field strength with a LeCroy 9384 digital oscilloscope and sent to a microcomputer, which calculated the ΔA. The magnetic field was changed by a constant increment (either 0.5, 1, or 5 mT depending on desired resolution). Because of the length of the sample runs (>5 h), a small amount of sample degradation was observed, resulting in a decrease in the triplet yield at zero field, $\Delta A(B = 0)$, over the course of the experiments. To compensate for this, the magnetic field was reset to $B = 0$ mT every five kinetic traces for increments of 5 mT and every three kinetic traces for increments of 0.5 mT and 1 mT and $\Delta A(B = 0)$ was plotted and fit with a polynomial or series of polynomials. These functions were used to calculate the relative triplet yield as a function of applied field strength. The relative triplet yield is thus

$$\frac{T}{T_0} = \frac{\Delta A(B)}{\Delta A(B = 0)} \tag{3}$$

The results presented are an average of two or more experiments conducted on separate days with freshly prepared samples.

Results and Discussion

Steady-State Spectrosopy and Electrochemistry. The photophysics of the 6ANI chromophore have been characterized previously in detail.[18,36] The electronic spectra of MeOAn-6ANI-NI and MeOAn-6ANI-Me$_2$Ph-NI in toluene exhibit a broad charge transfer (CT) absorption centered at 397 nm due to the 6ANI chromophore, and a second band displaying vibronic

structure at 343, 363, and 382 nm arising from $\pi-\pi^*$ transitions within the NI acceptor. The PI acceptor has no appreciable absorption in this spectral region, and therefore, the spectra of MeOAn-6ANI-PI and MeOAn-6ANI-Me$_2$Ph-PI are virtually identical to that of 6ANI. The ^{1*}6ANI state decays radiatively in toluene ($\phi_F = 0.92$), but its emission is quenched by photoinduced electron transfer to covalently attached electron donors or acceptors. Attachment of the MeOAn electron donor to 6ANI via a piperazine bridge results in strong quenching of the emission, consistent with the rapid electron-transfer reaction: MeOAn-^{1*}6ANI → MeOAn$^+$-6ANI$^-$, which occurs within this pair.[18]

The 6ANI chromophore undergoes reversible oxidation and reduction at modest potentials, which makes it well suited for use in covalently linked donor−acceptor molecules. The oxidation potential of 6ANI (1.2 V vs SCE) is similar to that of piperidine, whereas its reduction potential (−1.4 V vs SCE) is similar to that of naphthalene-1,8-dicarboximide.[37] The oxidation potential of the MeOAn electron donor (0.79 V) is substantially less positive than that of 6ANI because of resonance stabilization of the cation on the aniline moiety by the MeO group.[18,38] The first reduction potential of NI occurs at −0.5 V, and that of PI at −0.79 V.[39]

Radical Pair Spin Density and Donor−Acceptor Distance. Optimized ground-state geometries of MeOAn-6ANI-NI, MeOAn-6ANI-PI, MeOAn-6ANI-Me$_2$Ph-NI, and MeOAn-6ANI-Me$_2$Ph-PI were calculated using AM1 within Hyperchem 5.01.[40] The results show that, for MeOAn-6ANI-NI and MeOAn-6ANI-PI, the dihedral angle of the aromatic core of 6ANI relative to those of the NI and PI acceptors are 90° and 86°, respectively, so that the π systems of these subunits are essentially orthogonal to one another. In MeOAn-6ANI-Me$_2$Ph-NI and MeOAn-6ANI-Me$_2$Ph-PI, the dihedral angles between 6ANI and the Me$_2$Ph bridge are both 86°, whereas those between the Me$_2$Ph bridge and NI and PI are 82° and 72°, respectively. These data suggest that the amplitude of the torsional motion of PI about its bond to both 6ANI and Me$_2$Ph in these molecules is most likely larger than that of NI. This is a consequence of the reduced steric demand of the five-membered imide ring of PI relative to that of the six-membered imide ring of NI.

Unrestricted Hartree−Fock (UHF) molecular orbital calculations under the AM1 model were used to calculate the spin densities for the radical ions relevant to the four donor−acceptor molecules.[40] These unpaired spin densities for the radical ions are given in Chart 2. The spin in the radical cation is localized primarily on the *p*-methoxyphenyl group and the piperazine nitrogen atom closest to it. The unpaired spin densities for the radical anions of NI and PI are distributed symmetrically about their respective naphthalene and benzene rings. The effective radical pair distances listed in Table 1 are determined by

TABLE 1: Ion Pair Distances (r), Weighted by the Unpaired Spin Density Distributions of the Donor and Acceptor, Radical Ion Pair Energies (ΔG_{pRP} and ΔG_{RP}), Measured Charge Separation Rate Constants (k_{CS1} and k_{CS2}), Measured Spin−Spin Exchange Interaction ($2J$), Electronic Coupling Matrix Elements (V_{RP-pRP} and V_{CR}) Determined from the Experimental Data Using Equation 6, Charge Recombination Rate Constant (k_{CRS}) Calculated Using V_{CR} and ΔG_{RP2} and Equation 7, and the Experimentally Measured Charge Recombination Rate Constant (k_{CR})

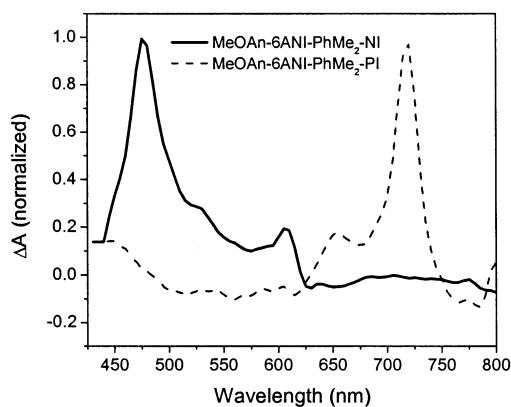| compound	r (Å)pRP	r (Å)RP	ΔG_{pRP} (eV)	ΔG_{RP} (eV)	k_{CS1} (s^{-1})	k_{CS2} (s^{-1})	$2J$ (mT)	V_{RP-pRP} (cm^{-1})	V_{CR} (cm^{-1})	k_{CRS} (s^{-1})	k_{CR} (s^{-1})
MeOAn-6ANI-NI	11.0	14.7	2.32	2.06	1.4×10^{12}	1.0×10^{11}	47.5	16.0	7.3	5.4×10^{4}	3.5×10^{7}
MeOAn-6ANI-PI	7.7	14.9	2.48	2.24	1.25×10^{11}	6.7×10^{10}	66.0	13.2	2.2	6.2×10^{2}	6.0×10^{7}
MeOAn-6ANI-Me$_2$Ph-NI	7.7	18.5	2.48	2.06	1.25×10^{11}	2.3×10^{9}	1.0	2.7	1.0	1.0×10^{3}	5.0×10^{6}
MeOAn-6ANI-Me$_2$Ph-PI	7.7	18.4	2.48	2.32	1.25×10^{11}	6.7×10^{10}	2.0 19.0	22.3	7.4	5.6×10^{3}	1.4×10^{7}

Figure 1. Transient absorption spectra of MeOAn-6ANI-Me$_2$-OPh-NI and MeOAn-6ANI-Me$_2$-Ph-PI at 64 and 52 ns, respectively, following excitation with a 416 nm, 7 ns laser flash.

Figure 2. Kinetic traces at 480 nm for compound MeOAn-6ANI-NI.

weighting the atomic distances obtained from energy-minimized structures with the calculated spin densities at the particular atoms.

Charge Recombination in the Absence of an External Magnetic Field. Previous work[18] has shown that photoexcitation of 6ANI within MeOAn-6ANI-Me$_2$Ph-NI results in the initial formation of the MeOAn$^+$-6ANI$^-$-Me$_2$Ph-NI radical pair with $\tau = 8$ ps, as detected by the presence of the 6ANI$^-$ anion radical, which has distinct absorptions at 420 nm ($\epsilon = 23\,500$ cm^{-1} M^{-1}) and 510 nm ($\epsilon = 7000$ cm^{-1} M^{-1}). Subsequently, there is a rapid secondary electron transfer to form the MeOAn$^+$-6ANI-Me$_2$Ph-NI$^-$ radical pair with $\tau = 430$ ps, detected by the presence of the NI$^-$ anion radical, which has distinct absorptions at 480 nm ($\epsilon = 28\,300$ cm^{-1} M^{-1}) and 605 nm ($\epsilon = 7000$ cm^{-1} M^{-1}).[39] A similar mechanism occurs following photoexcitation of 6ANI in MeOAn-6ANI-Me$_2$Ph-PI and MeOAn-6ANI-PI, where the initial MeOAn$^+$-6ANI$^-$ radical ion pair is formed with $\tau = 8$ ps, followed by a rapid charge shift to form MeOAn$^+$-6ANI-Me$_2$Ph-PI$^-$ and MeOAn$^+$-6ANI-PI$^-$ that occurs in both cases with $\tau = 15$ ps, as indicated by the presence of PI$^-$ ($\lambda_{max} = 700-720$ nm, $\epsilon = 41\,700$ cm^{-1} M^{-1}).[39] Charge separation within MeOAn-6ANI-NI proceeds by a slightly different mechanism. Following selective photoexcitation of 6ANI in MeOAn-6ANI-NI, an initial charge separation occurs to form MeOAn-6ANI$^+$-NI$^-$ with $\tau = 0.7$ ps followed by a rapid charge shift with $\tau = 10$ ps to yield MeOAn$^+$-6ANI-NI$^-$. The final radical ion pairs are long-lived in toluene with lifetimes from about 15−200 ns as indicated in Table 1.

The transient absorption spectra of MeOAn-6ANI-Me$_2$Ph-NI and MeOAn-6ANI-Me$_2$Ph-PI at 64 and 52 ns, respectively, following excitation with a 416 nm, 7 ns laser flash, are displayed in Figure 1. At these times, the transient spectrum of MeOAn-6ANI-Me$_2$Ph-NI displays sharp features at 480 and 605 nm characteristic of the MeOAn$^+$-6ANI-Me$_2$Ph-NI$^-$ radical pair,
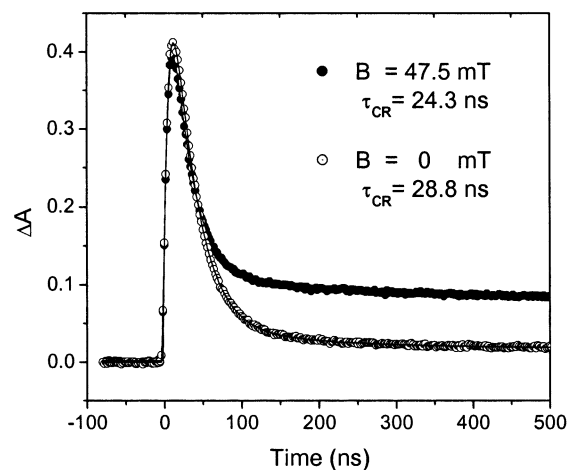
whereas that of MeOAn-6ANI-Me$_2$Ph-PI has a large 720 nm peak, characteristic of the MeOAn$^+$-6ANI-Me$_2$Ph-PI$^-$.[39] Each of these RPs is formed in a pure singlet state, which then mixes with the three triplet sublevels via the hyperfine and spin−spin exchange interactions. The transient optical absorption spectra of the singlet and triplet radical pair states are indistinguishable from one another; however, they undergo CR via quite different pathways. The singlet radical ion pair recombines to yield the ground state, which is the baseline within the transient absorption experiment, whereas the triplet radical ion pair recombines to yield the neutral triplet excited state. EPR measurements have shown that ^{3*}NI is the lowest excited triplet state in donor−acceptor molecules containing both 6ANI and NI, whereas ^{3*}6ANI is the lowest excited triplet state in molecules containing 6ANI and PI.[41,42] In either case, the triplet state of MeOAn is higher in energy and not observed.

The CR dynamics in MeOAn-6ANI-NI, MeOAn-6ANI-PI, MeOAn-6ANI-Me$_2$Ph-NI, and MeOAn-6ANI-Me$_2$Ph-PI are obtained by monitoring the NI$^-$ at 480 nm or PI$^-$ at 720 nm, whereas both ^{3*}NI and ^{3*}6ANI exhibit a broad optical absorption centered at 480 nm. For example, Figure 2 shows the nanosecond transient absorption kinetics for the decay of MeOAn$^+$-6ANI-NI$^-$. The transient kinetics at 480 nm are characterized by an instrument-limited rise followed by exponential decay to a much longer-lived absorption, which is due to the formation of MeOAn-6ANI-^{3*}NI. The rate constants for CR of the radical anions formed in MeOAn-6ANI-NI, MeOAn-6ANI-PI, MeOAn-6ANI-Me$_2$Ph-NI, and MeOAn-6ANI-Me$_2$-Ph-PI at $B = 0$ are given in Table 1. These rate constants are the sum of the rates for CR of the singlet and triplet radical pairs, labeled within Figure 3 as k_{CRS} and k_{CRT}, respectively. These rates are likely to differ considerably because of large differences in their free energies of reaction.
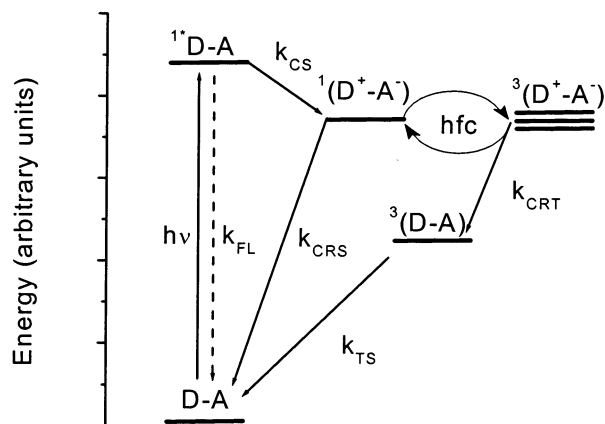
Direct Measurement of Singlet−Triplet Splitting

J. Phys. Chem. A, Vol. 107, No. 19, 2003 **3643**

Figure 3. Energy level diagram for relevant donor−acceptor electronic states.

Figure 4. Radical ion pair energy levels as a function of magnetic field.

Charge Recombination in the Presence of an External Magnetic Field. The spin Hamiltonian for radical pairs in solution is given by

$$H_{ST} = \beta B_0(g_1\mathbf{S}_1 + g_2\mathbf{S}_2) + \sum_i a_{1i}\mathbf{S}_1\cdot\mathbf{I}_i + \sum_k a_{2k}\mathbf{S}_2\cdot\mathbf{I}_k - 2J\mathbf{S}_1\cdot\mathbf{S}_2 \quad (4)$$

where β is the Bohr magneton, B_0 is the applied magnetic field, g_1 and g_2 are the electronic g factors for each radical, $\mathbf{S}_1$ and $\mathbf{S}_2$ are electron spin operators for the two radicals within the radical pair, $\mathbf{I}_i$ and $\mathbf{I}_k$ are nuclear spin operators, a_{1i} and a_{2k} are the isotropic hyperfine coupling constants of nucleus i with radical 1 and nucleus k with radical 2, and J is the scalar spin−spin exchange interaction constant. The small differences in g factors for organic radicals such as those studied here contribute to singlet−triplet mixing only at field strengths of several Tesla, so that the first term in eq 4 can be neglected for the systems studied here. Anisotropic exchange interactions and hyperfine couplings, as well as the magnetic dipole−dipole interaction, are neglected because the measurements are performed in solution. Also, it is assumed that nuclei associated structurally with a given radical couple only with the electron spin within that radical.

Immediately after charge separation, the correlated electron spins are in a singlet configuration. This pure state is, in general, not an eigenstate of H_{ST}, as the weakly coupled electron spins are free to precess independently around the resultant of their respective local fields and the external applied field. After times that are usually in the range of a few nanoseconds, spin dephasing results in formation of a triplet configuration. When hyperfine and exchange interactions are isotropic and spin−spin coupling is weak, each of the three zero-field triplet states of the radical pair will be nearly degenerate with the singlet and will be populated with equal probability. The Zeeman interaction results in splitting of triplet sublevels, which at high fields can be described by the S, T_0 and $T_{\pm 1}$ states as shown in Figure 4. In the high field limit, population of the radical pair triplet state occurs exclusively by S−T_0 mixing, whereas T_{-1} and T_{+1} remain unpopulated. If the spin−spin exchange interaction within the radical ion pair is nonzero, the triplet manifold is not initially degenerate with the singlet, but rather separated by an energy $2J$, Figure 4. EPR measurements on closely related compounds have confirmed that the triplet levels of the radical pair are higher in energy than the singlet state as would be expected from net antiferromagnetic exchange.[41] When the Zeeman energy from the applied field equals that of the
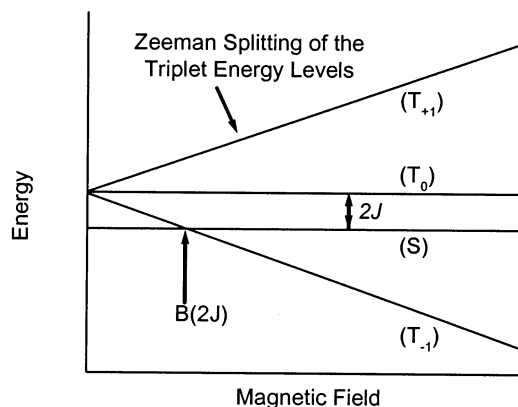
S−T splitting, the low energy triplet state, T_{-1}, crosses the singlet, and the radical pair intersystem crossing rate is maximized, which produces a so-called $2J$ resonance in the triplet yield. The magnitude of $2J$ and the line shape of the resonance both provide insights into the structural and electronic parameters that dictate the rate of charge recombination.

Figure 5 shows the magnetic field dependence of the yields of MeOAn-6ANI-³NI, MeOAn-³6ANI-PI, MeOAn-6ANI-Me₂-Ph-³NI, and MeOAn-³6ANI-Me₂Ph-PI formed by RP-ISC followed by charge recombination. The triplet yields for compounds MeOAn-6ANI-NI and MeOAn-6ANI-PI, Figure 5, parts a and b, the directly linked donor−acceptor systems, exhibit resonances at 47. 5 and 66 mT, respectively. Inserting the Me₂Ph spacer results in a significant decrease in the magnitude of $2J$. The triplet yield for MeOAn-6ANI-Me₂Ph-NI displays a resonance at 1 mT (Figure 5c), which is on the order of the hyperfine interaction. A similar very low field resonance is observed for MeOAn-6ANI-Me₂Ph-PI (Figure 5d) at 2 mT, which also clearly displays a second resonance at $B(2J)$ = 19 mT.

Energy of the 2J Resonance and the Electronic Coupling Magnitude. The energy at which the $2J$ resonance occurs equals the energy splitting between singlet and triplet configurations of the RP.[43] Both the magnitude and sign of $2J$ depend on interactions between the singlet and triplet RP states with other energetically nearby states having the same respective spin multiplicities. Thus, eq 1 can be truncated to four terms that relate $2J$ to the electronic coupling matrix elements that connect the singlet RP state to its precursor singlet RP state (pRP) and the singlet ground state, and the triplet RP state to ³*6ANI and ³*NI or ³*PI

$$2J = \left[\frac{|V_{RP-GS}|^2}{\Delta E_{RP-GS}} + \frac{|V_{RP-pRP}|^2}{\Delta E_{RP-pRP}}\right] - \left[\frac{|V_{RP-³*6ANI}|^2}{\Delta E_{RP-³*6ANI}} + \frac{|V_{RP-³*A}|^2}{\Delta E_{RP-³*A}}\right] \quad (5)$$

where A = NI or PI. The energies of the pRP states are given in Table 1, and those of ³*6ANI and ³*NI or ³*PI are 2.05,[18] 2.03,[18] and 2.45 eV,[42] respectively. The relevant pRP states are MeOAn⁺-6ANI⁻ for MeOAn-6ANI-Me2Ph-NI, MeOAn-6ANI-Me2Ph-PI, and MeOAn-6ANI-PI, as well as 6ANI⁺-NI⁻ for MeOAn-6ANI-NI.

We assume, as has been done previously,[4−6] that the electronic coupling matrix elements for charge recombination to ³*6ANI, ³*NI, and the singlet ground state are approximately equal (V_{CR}) because of similarities in the charge distributions
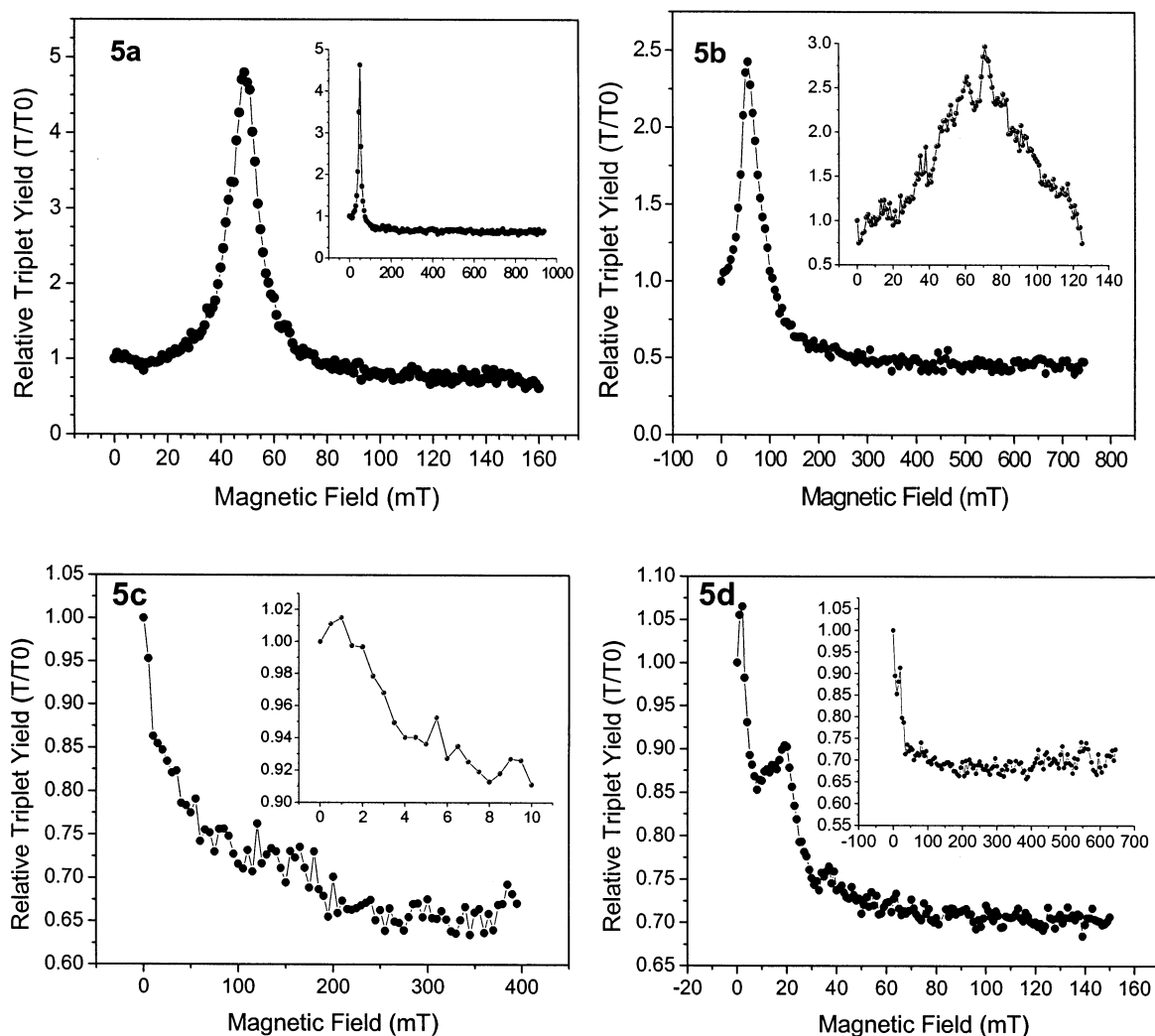
Figure 5. Triplet yields as a function of magnetic field for (a) MeOAn-6ANI-NI; (b) MeOAn-6ANI-PI; (c) MeOAn-6ANI-Me$_2$Ph-NI; and (d) MeOAn-6ANI-Me$_2$Ph-PI. The insets provide expanded or contracted views of the data.

of the initial and final states as well as the relatively large distance between the radical ions within the pair. Thus, the last three terms of eq 5 can be combined to yield eq 6:

$$2J = \frac{|V_{RP-pRP}|^2}{\Delta E_{RP-pRP}} -$$
$$|V_{CR}|^2\left(\frac{1}{\Delta E_{RP-GS}} + \frac{1}{\Delta E_{RP-3*6ANI}} + \frac{1}{\Delta E_{RP-3*A}}\right) \quad (6)$$

Equation 6 is used to estimate V_{CR}. The radical ion pair energies for each compound used to calculate the energy denominators in eq 6 are obtained using the spectroscopic method outlined by Greenfield et al.[18] The value of $\lambda_I = 0.3$ eV is assumed to be identical for each compound in the series and the calculated values of the free energies are listed in Table 1. From the Marcus formulation for solvent reorganization energy based on the Born dielectric continuum model of the solvent, $\lambda_S = 0.044$ eV for these compounds in toluene ($\epsilon_S = 2.38$ and $\epsilon_0 = 2.24$).[44] The solvent reorganization energy is small and nearly distance independent over the range of radical ion pair distances within the four compounds studied here. These quantities were used to calculate each energy denominator in eq 6 for each compound and are listed in Table 1.

Because the rate constants for the charge shift reactions that produce RP from pRP are all too fast to allow a significant

degree of singlet−triplet mixing in pRP, the charge shift reactions proceed exclusively through the singlet radical pairs. Thus, the value of V_{RP-pRP} is obtained from the standard expression from semiclassical electron transfer theory (valid for one quantum mode),[45−47] eq 7, using the measured rate constant k_{CS2}

$$k_{CS2} = \frac{2\pi}{\hbar}|V_{RP-pRP}|^2\sqrt{\frac{1}{4\pi\lambda_S k_B T}}\sum_{n=0}^{\infty}\exp(-S)\frac{S^n}{n!} \times$$
$$\exp\left[\frac{-((\Delta G_{CS2} - \Delta G_{CS1}) + \lambda_S + n\hbar\omega)^2}{4\lambda_S k_B T}\right] \quad (7)$$

In eq 7, $\hbar\omega$ is the vibrational quantum, assumed to be 1500 cm^{-1}, $S = \lambda_I/\hbar\omega$, where λ_I is the internal reorganization energy of the donor−acceptor molecule and λ_S is the solvent reorganization energy, and ($\Delta G_{CS2} - \Delta G_{CS1}$) is the free energy difference between the RP and pRP states. The summation n is done over the quantum number of the high-frequency vibrational mode (truncated here at $n = 15$). The values of V_{RP-pRP} obtained from eq 7 are given in Table 1. Using these data and the experimental values of $2J$, eq 6 is used to calculate V_{CR}, which is also given in Table 1. The measured rate constant for charge recombination, k_{CR}, is the sum of the rate constants for charge

Direct Measurement of Singlet−Triplet Splitting

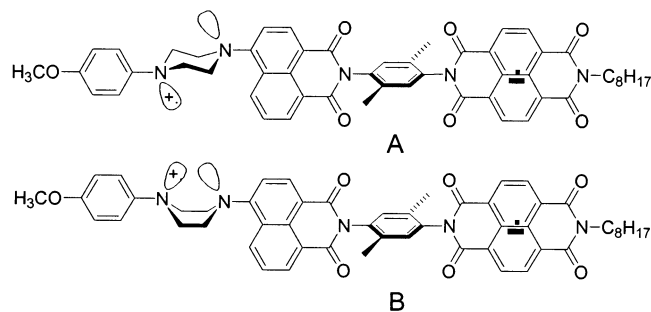*J. Phys. Chem. A, Vol. 107, No. 19, 2003* **3645**

Figure 6. Two conformations of MeOAn⁺-6ANI-Ph-NI⁻ resulting from chair-boat inversion of the piperazine ring.

recombination to the local excited triplet state, k_{CRT}, as well as the ground state, k_{CRS}. The values for V_{CR} and ΔG_{CR2} are used in eq 7 to estimate k_{CRS}, Table 1. The predicted values of k_{CRS} are substantially smaller than the experimental values of k_{CR}. From these numbers, it is clear that the RP recombination rate is dominated by recombination of the triplet RP to the localized triplet(s) in each of these molecules.

The spin−spin exchange interaction is also strongly dependent on the distance between the spins:[33]

$$2J = 2J_0 e^{-\alpha(r_{DA} - r_0)} \quad (8)$$

where $2J$ is the observed resonance, r_{DA} is the radical pair separation, r_0 is the van der Waals contact distance of 3.4 Å, $2J_0$ is the spin−spin exchange interaction at r_0, and α is a system specific decay parameter. The values of V_{CR} calculated for MeOAn⁺-6ANI-NI⁻ and MeOAn⁺-6ANI-Me₂Ph-NI⁻, 7.3 and 1.0 cm⁻¹, respectively, are consistent with the increase in distance that results from placing Me₂Ph spacer between 6ANI and NI. However, the opposite ordering for V_{CR} is calculated for MeOAn⁺-6ANI-PI⁻ and MeOAn⁺-6ANI-Me₂Ph-PI⁻, where V_{CR} = 2.2 and 7.4 cm⁻¹, respectively. The larger coupling for MeOAn⁺-6ANI-Me₂Ph-PI⁻ may be due to greater overlap of the π systems of PI and the Me₂Ph spacer as indicated by the smaller calculated dihedral angle between them (72°) relative to that between NI and Me₂Ph (82°), as noted above.

The appearance of two resonances within MeOAn-6ANI-Me₂-Ph-PI most likely results from two populations of molecules which each have slightly different radical ion pair distances or orientations. One possible source of two conformations within the radical ion pair is a chair ↔ boat interconversion of the piperazine ring, Figure 6. The radical ion pair distance is reduced slightly in the boat conformation (B) resulting in additional Coulombic stabilization of the radical ion pair. Conformational changes resulting from Coulombic attraction of the ions, i.e., "harpooning", have been observed in related photogenerated radical ion pairs.[48] Our data support a relatively small structural change due to this mechanism. Larger structural changes, such as those proposed to explain earlier observations, are not likely in our molecules because folding the MeOAn⁺ radical cation over 6ANI decreases r_{DA} to much smaller values that would produce a second resonance at much higher fields, which is not observed. Earlier work also suggests that deviations from a zigzag arrangement of saturated bonds diminishes the through-bond coupling for electron-transfer reactions.[49,50] However, the transannular interaction of the nitrogen lone pair orbitals depicted in Figure 6, structure B, most likely provides an additional pathway to enhance V_{CR} that may compensate for the decrease in coupling expected from the orientation of the C−C bonds in the boat conformation. A balance between these two opposing effects is consistent with the modest $2J$ = 19 mT

TABLE 2: 2J Values, Hyperfine Energies, and Observed Resonance Linewidths

compound	2J (mT)	ΔB (mT) (fwhm)	ΔB_HFI (mT)
MeOAn-6ANI-NI	47.5	15.1	2.6
MeOAn-6ANI-PI	66.0	46.3	2.7
MeOAn-6ANI-Me₂Ph-NI	1.0	9.0	2.6
MeOAn-6ANI-Me₂Ph-PI	2.0, 19.0	3.7, 6.3	2.7

value of the second resonance for MeOAn-6ANI-Me₂Ph-PI. An important question arises as to why two resonances are not observed for the other three molecules. This question will be addressed in the next section that deals with the resonance line shapes.

Line Shape of the 2J Resonance. For the radical pair lifetimes observed here (>15 ns), lifetime broadening does not contribute significantly to the overall line shape of the magnetic field response, so that other interactions are responsible for the observed variations in line shape.[51] Weller developed an approximate treatment that describes the contribution of the electron−nuclear hyperfine interactions due to the magnetic nuclei on each radical center to the overall line shape of the magnetic field effect.[52] This treatment uses the root-mean-square value of all of the hyperfine interactions on a particular radical given by

$$B_i = \left[\sum_k I_k(I_k + 1)a_{ik}^2 \right]^{1/2} \quad (9)$$

where a_{ik} are the values of the isotropic hyperfine coupling constants between the nuclear spins I_k and the unpaired electron on radical i. The width of each of the singlet and triplet sublevels as a result of hyperfine coupling is approximated by the weighted sum of the hyperfine contributions at both radicals

$$\Delta B_{HFI} = 2\frac{B_1^2 + B_2^2}{B_1 + B_2} \quad (10)$$

This interaction contributes a width of ΔB_{HFI} to the spin states. ΔB_{HFI} calculated for each of the compounds studied here is given in Table 2, along with the fwhm of the observed resonances.[53−57] It is immediately clear from the data in Table 2 that the hyperfine interaction is not principally responsible for the observed line widths of the 2J resonances in these systems.

Thus, we must consider other sources of broadening, such as modulation of the 2J value by internal motions within the covalently linked radical ion pair. Although changes in the spin distribution primarily change the overall effective radical ion pair distance, r_{DA}, changes in the interaction of the spin distributions of the radical ions with the intervening orbitals connecting the two radicals may create significant dispersion in the value of $2J_0$ (eq 8) even within a series of structurally related radical ion pairs. The principal internal molecular motions available to the four molecules studied here are torsional motions about the single bonds joining MeOAn to 6ANI, 6ANI to either NI or PI, and the corresponding motions involving junctions to the Me₂Ph spacer. In addition, chair ↔ boat interconversion involving the piperazine is also possible.

Our molecular orbital calculations of the ground states of all four molecules suggest that the amplitude of the torsional motion of PI is most likely larger than that of NI when they are attached either directly to 6ANI or to the Me₂Ph spacer. This may result in an increase in line width of the 2J resonance as a consequence of modulating the spin−spin interaction between the two radical

ions on a time scale that corresponds to $2J$. The torsional motions of the piperazine ring relative to the naphthalene-1,8-dicarboximide in 6ANI and those of Me$_2$Ph relative to that of 6ANI are assumed to be constant in this series of molecules because the charge (and spin) densities of the radical ions are distributed at sites far removed from these centers. The only remaining motion that may have a significant impact on the line widths of the $2J$ resonances is the chair ↔ boat interconversion of the piperazine ring. This motion will impact how MeOAn$^+$ interacts electronically with the rest of the intervening structure between the two radical ions. If the chair ↔ boat interconversion of the piperazine ring is the source of the two resonances observed for MeOAn-6ANI-Me$_2$Ph-PI, there is no obvious reason the remaining three molecules should not exhibit similar conformational diversity at their piperazine rings and thus two resonances. An examination of the line widths of the resonances exhibited by the other molecules shows that the full width at half-maximum (fwhm) of the resonances for MeOAn-6ANI-PI and MeOAn-6ANI-NI are 46.3 mT and 15.1 mT, respectively, whereas those for the two resonances for MeOAn-6ANI-Me$_2$Ph-PI are only 3.7 and 6.3 mT, and that for the single resonance of MeOAn-6ANI-Me$_2$Ph-NI is only 9.0 mT. Thus, the narrower line widths of the resonances in MeOAn-6ANI-Me$_2$Ph-PI make it possible to resolve, albeit incompletely, two resonances that differ by only 17 mT. However, the 9.0 mT line width of the single resonance of MeOAn-6ANI-Me$_2$Ph-NI may not be sufficiently narrow to resolve the second resonance given our current signal-to-noise. A careful examination of the line shape in Figure 5c hints at the possibility of a second line due to the breadth of the signal at about 25 mT. The corresponding resonances are unresolved for the substantially broader lines in MeOAn-6ANI-PI and MeOAn-6ANI-NI.

The possibility of two conformations, however, does not ensure the observation of two distinct $2J$ resonances. To observe distinct resonances, the time constant for interconversion must be slow relative to the energy difference between the resonances. The difference in $2J$ values within MeOAn-6ANI-Ph-PI is 17 mT, which corresponds to a transform limited time of approximately 0.3 ns. Thus, interconversion of the A and B conformers, if it does occur, must occur at times slower than 0.3 ns to observe distinct resonances. From the amplitude of the two resonances, there appears to be a preference for the A conformation with the longer distance. However, it must be remembered that for such small $2J$ values, HFIs play a significant role in driving RP–ISC. Although both resonances within MeOAn$^+$-6ANI-Me$_2$Ph-PI$^-$ have contributions from hyperfine and exchange interactions, the relative magnitude of HFI is significantly greater at the lower field resonance. Therefore, the amplitudes of the two resonances do not necessarily reflect the relative populations of the two radical ion pair conformations.

Conclusions

We have shown that the dependence of the triplet yield derived from radical pair intersystem crossing on an applied magnetic field can be used to determine directly the singlet–triplet splitting between the radical ions in rodlike covalently linked, photogenerated radical ion pairs. The value of $2J$ is a sensitive probe of the dependence of the dominant electronic coupling matrix elements (in this case, those which dictate charge recombination to the localized triplet excited states) on molecular structure. Moreover, the line shape of the $2J$ resonance can be analyzed with respect to local hyperfine interactions, the degree of charge delocalization on each radical center, and

molecular structure. It is evident that despite the significant degree of conformational control that these rodlike structures afford, there remain important intramolecular motions that modulate the overall electronic coupling between the radical ions. These small variations in structure can have significant impact on the rates of charge recombination. The direct connection made between radical ion pair structure and the characteristics of the $2J$ resonance in the systems presented here suggests that this methodology shows great potential for the elucidation of electronic coupling factors for nonadiabatic electron transfer in more complex systems.

Supporting Information Available: Synthesis and characterization of compounds MeOAn-6ANI-NI and MeOAn-6ANI-Me$_2$Ph-PI. This material is available free of charge via the Internet at http://pubs.acs.org.

References and Notes

(1) Anderson, P. W. *Phys. Rev.* **1959**, *115*, 2−13.
(2) Soos, Z. *Annu. Rev. Phys. Chem.* **1974**, *25*, 121−153.
(3) Okamura, M. Y.; Isaacson, R. A.; Feher, G. *Biochim. Biophys. Acta* **1979**, *546*, 394.
(4) Marcus, R. A. *Chem. Phys. Lett.* **1987**, *133*, 471−477.
(5) Bixon, M.; Jortner, J.; Michel-Beyerle, M. E. *Z. Phys. Chem. NF* **1993**, *180*, 193−208.
(6) Volk, M.; Haberle, T.; Feick, R.; Ogrodnik, A.; Michel-Beyerle, M. E. *J. Phys. Chem.* **1993**, *97*, 9831−9836.
(7) Nelsen, S. F.; Ismagilov, R. F.; Teki, Y. *J. Am. Chem. Soc.* **1998**, *120*, 2200−2201.
(8) Kobori, Y.; Sekiguchi, S.; Akiyama, K.; Tero-Kubota, S. *J. Phys. Chem. A* **1999**, *103*, 5416−5424.
(9) Yago, T.; Kobori, Y.; Akiyama, K.; Tero-Kubota, S. *J. Phys. Chem. B* **2002**, *106*, 10074−10081.
(10) Kakitani, T.; Matsuda, N.; Yoshimori, A.; Mataga, N. *Prog. React. Kinet.* **1995**, *20*, 347−381.
(11) Kharkats, Y.; Ulstrup, J. *Chem. Phys. Lett.* **1991**, *182*, 81−87.
(12) Kumar, K.; Lin, Z.; Waldeck, D.; Zimmt, M. B. *J. Am. Chem. Soc.* **1996**, *118*, 243−244.
(13) Lopez-Castillo, J.-M.; Filali-Mouhim, A.; Jay-Gerin, J.-P. *J. Phys. Chem.* **1993**, *97*, 9266−9269.
(14) Lopez-Castillo, J.-M.; Filali-Mouhim, A.; Jay-Gerin, J.-P. *Chem. Phys. Lett.* **1995**, *239*, 223−229.
(15) Lopez-Castillo, J.-M.; Filali-Mouhim, A.; Plante, I. L.; Jay-Gerin, J.-P. *J. Phys. Chem.* **1995**, *99*, 6864−6875.
(16) Lopez-Castillo, J.-M.; Jay-Gerin, J.-P. *J. Phys. Chem.* **1996**, *100*, 0.
(17) Kurnikov, I.; Beratan, D. *J. Chem. Phys.* **1996**, *105*, 9561−9573.
(18) Greenfield, S. R.; Svec, W. A.; Gosztola, D. J.; Wasielewski, M. R. *J. Am. Chem. Soc.* **1996**, *118*, 6767−6777.
(19) Haberkorn, R.; Michel-Beyerle, M. E.; Marcus, R. *Proc. Natl. Acad. Sci. U.S.A.* **1979**, *76*, 4185−4188.
(20) Blankenship, R. E. *Acc. Chem. Res.* **1981**, *14*, 163−170.
(21) Blankenship, R. E.; Schaafsma, T. J.; Parson, W. W. *Biochim. Biophys. Acta* **1977**, *461*, 297−305.
(22) Ciminale, F.; Curci, R.; Portacci, M.; Troisi, L. *Tetrahedron Lett.* **1988**, *29*, 2463−2466.
(23) Closs, G. L.; Forbes, M. D. E.; Norris, J. *J. Phys. Chem.* **1987**, *91*, 3592−3599.
(24) Haberkorn, R.; Michel-Beyerle, M. E. *Biophys. J.* **1979**, *26*, 489−498.
(25) Hoff, A. J. *Photochem. Photobiol.* **1986**, *43*, 727−745.
(26) Hoff, A. J.; Rademaker, H.; Van Grondelle, R.; Duysens, L. N. M. *Biochim. Biophys. Acta* **1977**, *460*, 547−554.
(27) Hore, P. J.; Hunter, D. A.; McKie, C. D. *Chem. Phys. Lett.* **1987**, *137*, 495−500.
(28) Kingma, H.; Van Grondelle, R.; Duysens, L. N. M. *Biochim. Biophys. Acta* **1985**, *808*, 383−399.
(29) Michel-Beyerle, M. E.; Scheer, H.; Seidlitz, H.; Tempus, D. *FEBS Lett.* **1979**, *110*, 129−132.

(30) Schulten, K.; Staerk, H.; Weller, A.; Werner, H.; Nickel, B. Z. *Phys. Chem. NF* **1976**, *101*, 371–390.

(31) Till, U.; Hore, P. J. *Mol. Phys.* **1997**, *90*, 289–296.

(32) Wegner, M.; Fischer, H.; Grosse, S.; H.-M., V.; Oliver, A. M.; Paddon-Row, M. N. *Chem. Phys.* **2001**, *264*, 341–353.

(33) Weller, A.; Staerk, H.; Treichel, R. *Faraday Discuss. Chem. Soc.* **1984**, *78*, 271–278.

(34) Sinks, L. E.; Wasielewski, M. R. *J. Phys. Chem. A* **2003**, *107*, 611–620.

(35) Lukas, A. S.; Miller, S. E.; Wasielewski, M. R. *J. Phys. Chem.* **2000**, *104*, 931–940.

(36) Debreczeny, M. P.; Svec, W. A.; Marsh, E.; Wasielewski, M. R. *J. Am. Chem. Soc.* **1996**, *118*, 8174–8175.

(37) Gosztola, D.; Niemczyk, M. P.; Svec, W. A.; Lukas, A. S.; Wasielewski, M. R. *J. Phys. Chem. A* **2000**, *104*, 6545–6551.

(38) Debreczeny, M. P.; Svec, W.; Wasielewski, M. R. *New J. Chem.* **1996**, *20*, 815–828.

(39) Wiederrecht, G. P.; Niemczyk, M.; Svec, W.; Wasielewski, M. R. *J. Am. Chem. Soc.* **1996**, *118*, 8.

(40) AM1 calculations were performed using HyperChem(TM); Hypercube, Inc.: Gainesville, FL.

(41) Hasharoni, K.; Levanon, H.; Greenfield, S. R.; Gosztola, D. J.; Svec, W. A.; Wasielewski, M. R. *J. Am. Chem. Soc.* **1995**, *117*, 8055–8056.

(42) Wiederrecht, G. P.; Svec, W. A.; Wasielewski, M. R.; Galili, T.; Levanon, H. *J. Am. Chem. Soc.* **2000**, *122*, 9715–9722.

(43) Sutin, N. *Prog. Inorg. Chem.* **1983**, *30*, 441–499.

(44) Marcus, R. A.; Sutin, N. *Biochim. Biophys. Acta* **1985**, *811*, 265–322.

(45) Hopfield, J. J. *Proc. Natl. Acad. Sci. U.S.A.* **1974**, *71*, 3640–3644.

(46) Jortner, J. *J. Chem. Phys.* **1976**, *64*, 4860–4867.

(47) Marcus, R. *J. Chem. Phys.* **1984**, *81*, 4494–4500.

(48) Lauteslager, X. Y.; van Stokkum, I. H. M.; van Ramesdonk, H. J.; Brouwer, A. M.; Verhoeven, J. W. *J. Phys. Chem. A* **1999**, *103*, 653–659.

(49) Oliver, A. M.; Craig, D. C.; Paddon-Row, M. N.; Kroon, J.; Verhoeven, J. W. *Chem. Phys. Lett.* **1988**, *150*, 366–373.

(50) Wasielewski, M. R.; Niemczyk, M. P.; Johnson, D. G.; Svec, W. A.; Minsek, D. W. *Tetrahedron* **1989**, *45*, 4785–4806.

(51) Staerk, H.; Treichel, R.; Weller, A. *Chem. Phys. Lett.* **1983**, *96*, 28–30.

(52) Weller, A.; Nolting, F.; Staerk, H. *Chem. Phys. Lett.* **1983**, *96*, 24–27.

(53) Heinen, U.; Berthold, T.; Kothe, G.; Stavitski, E.; Galili, T.; Levanon, H.; Wiederrecht, G.; Wasielewski, M. R. *J. Phys. Chem. A* **2002**, *106*, 1933–1937.

(54) Ciminale, F.; Curci, R.; Portacci, M.; Troisi, L. *Tetrahedron Lett.* **1988**, *29*, 2463–2466.

(55) Kiefer, A. M.; Kast, S. M.; Wasielewski, M. R.; Laukermann, K.; Kothe, G. *J. Am. Chem. Soc.* **1999**, *121*, 188–198.

(56) Zhong, C. J.; Kwan, W. S. V.; Miller, L. L. *Chem. Mater.* **1992**, *4*, 1423–1428.

(57) Nelsen, S. F. *J. Am. Chem. Soc.* **1967**, *89*, 5925.